2010

Development of an Advanced Radiation Exchange Module for Use in Simulation of Spaces with Radiant Systems

Devin Matthew Rohan
Purdue School of Civil Engineering

Athanasios Tzempelikos
Purdue School of Civil Engineering

William Travis Horton
Purdue School of Civil Engineering

Development of an Advanced Radiation Exchange Module for Use in Simulation of Spaces with Radiant Systems

Devin M. ROHAN[1], Athanasios TZEMPELIKOS[2,*], W. Travis HORTON[3]

School of Civil Engineering, Purdue University, West Lafayette, Indiana, USA

[1]Tel.: 574-229-4164, E-mail: drohan@purdue.edu
[2]Tel: 765-496-7586, E-mail: ttzempel@purdue.edu
[3]Tel.: 765-494-6098, E-mail: wthorton@purdue.edu

* Corresponding Author

ABSTRACT

The surface temperature of radiant systems can be significantly different than the temperature of other room surfaces; therefore, radiation heat exchange often becomes the dominant mode of heat transfer. It is necessary to accurately predict the surface temperature of radiant systems and to model radiative heat fluxes in detail, in order to evaluate the thermal environment and the impact on energy and comfort. This paper presents the development of a radiation exchange module that can be used to predict the performance of rooms with radiant systems with and without the presence of solar radiation. The module is based on radiosity theory in enclosures and includes detailed computation of window projections of the floor (sunlit area) which are treated a separate surface in an 8-surface enclosure. A comparison between heat fluxes calculated with currently accepted models (i.e. constant, linearized, and non-linear heat transfer coefficients) and with the developed model is presented for variable surface temperature differences.

1. INTRODUCTION

Radiant floor heating and cooling systems are becoming increasingly popular, due to their ability to provide better thermal comfort than forced air systems. In addition, when coupled with a thermal mass storage system, this type of heating and cooling can significantly reduce energy consumption. Since the floor temperature can differ greatly from other surfaces in a room, radiative heat exchange can become the predominant mode of heat transfer. It then becomes important to accurately predict the surface temperatures within the room and model the radiative heat fluxes, in order to evaluate thermal comfort within the room, energy consumption, and optimal control of the radiant heating system.

Numerous studies have been performed, documenting the performance, design, and control of radiant systems. Scheatzle (2006) reported the performance of low mass radiant ceiling panels used for cooling and a high mass floor system for heating, which the results could be used to aid development in radiant simulation models. Olsen (2008) provides basic design parameters of radiant floor heating and cooling systems like: typical radiant heat exchange coefficients, tube spacing, flow rates, and operative temperature limits. Hanibuchi and Hokoi (1998) reported that floor heating produced almost uniform air temperature distributions, except near windows, and that the heating efficiency of the floor system is slightly dependent upon the placement within the room and the usable area. Athienitis and Chen (2000) performed a detailed numerical investigation on the effects of solar radiation and the transient heat transfer in floor heating systems. Experimental and simulation results showed the temperature of the localized sunlit area incident on the floor, in the test room, could be 8°C higher than other room surfaces.

The objective of this study is to compare the percent differences between radiative heat fluxes calculated from the following commonly used radiative heat transfer models:

(i) Constant radiative heat transfer coefficients;
(ii) Linearized (mean temperature cubed) and one emissivity value;
(iii) Non-linear coefficients with approximated emissivity factors (used for long parallel surfaces);
(iv) Non-linear coefficients with multiplied emissivities;
(v) The full radiosity method for building enclosures

The developed model calculates the radiative heat fluxes for a rectangular room with one window, while considering the sunlit floor area (window projection) as an extra surface, resulting in an 8-surface enclosure. The radiosity method includes detailed incoming and outgoing radiant flux computation for each of the 8 surfaces.

2. METHODOLOGY

2.1 Building Description

The first task in creating a dynamic radiative heat transfer model is to define the room geometry and window placement on the building's façade. A commercially available software package was used to define the model dimensions and carry out all subsequent calculations. The simulated space presented in this paper was a simple 4x4x3 m high room with a south-facing window.

2.2 Window Projection

Following the construction of the geometry, solar angle calculations were performed to determine the solar altitude and solar azimuth. These angles were then used to determine the sunlit projection of the window onto the floor. The localized surface temperature of this directly illuminated part can significantly increase, thus affecting heat exchange and, subsequently, dynamic control operation and thermal comfort.
The case where the sunlit projection is fully incident on the floor is shown in Figure 1.

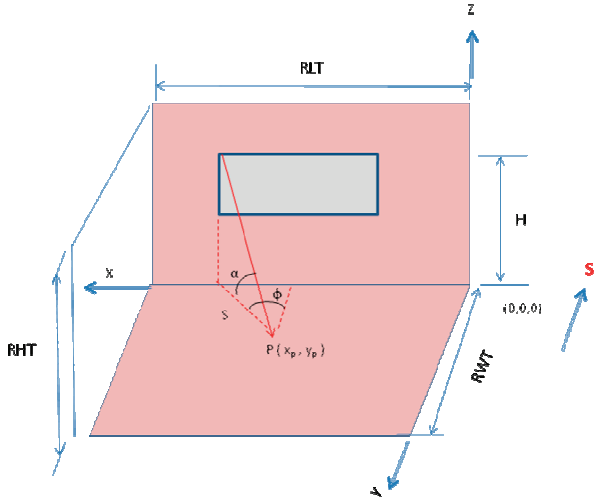

Figure 1: Window Sunlit Projection Incident on Floor.

The solar altitude angle (a) and the window height (H) were used to determine the depth of each window vertice (along the y-axis):

$$S = \frac{H}{\tan \alpha} \tag{1}$$

The solar azimuth angle can then be used to determine the offset along the room's width and depth from the window vertex positions. The x and y offset lengths from the window vertices can be calculated from equations (2) and (3) respectfully.

$$X = S \cdot \sin(\phi) \tag{2}$$

$$Y = S \cdot \cos(\phi) \tag{3}$$

where ϕ is the solar azimuth angle. For the general case that the façade is not facing true south, then the surface orientation has to be subtracted from the solar azimuth angle (to obtain the so-called "surface solar azimuth"). In this case, it is the angle from the solar ray projection on the floor and normal to the window wall surface. Once these lengths are known, equation (2) is added to the x-coordinate of each window vertice, since the solar azimuth is

negative in the morning and positive in the evening. This results in a sunlit projection left of the window and sweeping to the right as the day progresses, when viewed from outside of the building. Equation (3) is the y-coordinate of the sunlit projection on the floor and does not need to be modified like the *x* position. It should be noted that the sunlit projection crosses outside the bounds of the building dimensions, meaning the projection is incident upon left, right, or back walls at certain instances. When this occurred, the projection side was set to lay on the edge of the floor meeting the other vertical walls.

2.3 Window Projection Transformation

Once the sunlit projection on the floor is determined, it was transformed into an approximate rectangle of equal area, which is displayed in Figure 2.

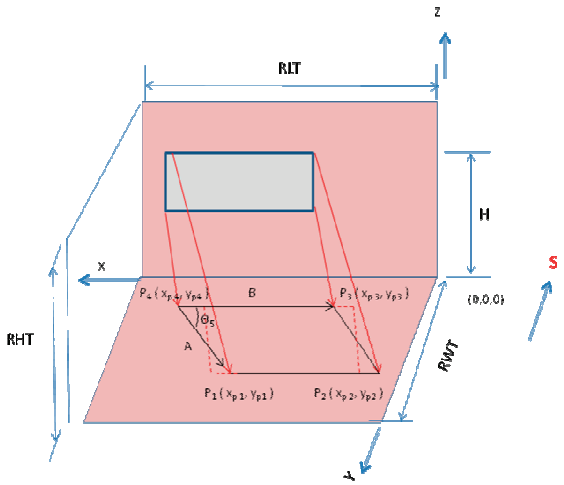

Figure 2: Transformation of window sunlit projection into an equivalent rectangle.

This provides the opportunity to use simplified view factors, which will be discussed shortly. The angle between vectors A and B (projection sides in Fig. 2) is first computed:

$$\cos(\theta_5) = \frac{\vec{A} \cdot \vec{B}}{|A||B|} \tag{4}$$

The midpoint of vector A was taken as half the length of vector A. The next step was to compute the shift in the x coordinate:

$$X_5 = \frac{|A|}{2} \cdot \cos(\theta_5) \tag{5}$$

The distance computed in equation (5) is added to the previously determined x-coordinate of points P_4 and P_3. Finally, in order to simplify calculations and increase computational speed,, the x-coordinates of points P_1 and P_2 were then set equal to those of points P_4 and P_3.

2.4 Radiative Heat Transfer Models

After the sunlit projection on the floor was determined, the view factors between all surfaces can be calculated, which represent the fractions of radiation leaving each surface and intercepted by any other surface. In addition to the room's six walls, the window and sunlit projection were treated as surfaces, resulting in an eight-sided enclosure (and a total of 64 view factors). After all view factors were determined, four separate models were utilized to find out the relative errors in radiative heat transfer, compared to the more robust full radiosity method. The first model uses a radiation heat transfer coefficient of hr = 5.6 W/m^2-^{o}K, which is assumed constant in most applications of low temperature heating (Causone *et al.* 2009) and in several simplified building thermal models. The resulting radiative heat flux is given by:

$$\dot{q}_{ij} = h_r \cdot F_{ij} \cdot \left(T_i - T_j\right) \tag{6}$$

where F_{ij} is the view factor between surface i and surface j and T_i and T_j are the temperatures of surface i and surface j respectively (in degrees Kelvin). The second model uses linearized heat transfer coefficients, which are equal to:

$$h_r = 4 \cdot \varepsilon \cdot \sigma \cdot \left(\frac{T_i - T_j}{2}\right)^3 \tag{7}$$

where ε is the surface emissivity and σ is the Stefan-Boltzmann constant. The next method utilizes a non-linear heat transfer coefficient, shown in Equation (8). Although it eliminates inaccuracies due to linearization, this method approximates the emissivity factor and stems from the heat transfer between two infinitely long planes.

$$h_r = \frac{\sigma \cdot \left(T_i^4 - T_j^4\right)}{\left(\frac{1}{\varepsilon_1} + \frac{1}{\varepsilon_2} - 1\right) \cdot \left(T_i - T_j\right)} \tag{8}$$

Finally, the last "simplified" method is similar to the non-linear coefficients but a simple emissivity factor is only used:

$$h_r = \frac{\sigma \cdot \varepsilon_i \cdot \left(T_i^4 - T_j^4\right)}{\left(T_i - T_j\right)} \tag{9}$$

The radiative coefficients from Equations 7, 8 and 9 were substituted into Equation (6) for calculation of heat fluxes and comparison of results. The radiosity method described in Siegel and Howell (1972) was used to determine the final heat flux of all (N) interior surfaces after theoretically infinite "inter-reflections". The full radiosity equation is shown in Equation (10).

$$C_k = \sum_{j=1}^{N} a_{kj} q_{o,j} \tag{10}$$

where $q_{o,j}$ is the radiosity of surface j and C_k is equal to:

$$C_k = \varepsilon_k \cdot \sigma \cdot T_k^4 \tag{11}$$

since it is assumed that temperatures can be specified. In addition, a_{kj} is defined as:

$$a_{kj} = \delta_{kj} - \left(1 - \varepsilon_k\right) F_{kj} \tag{12}$$

where δ_{kj}=1 when k=j and δ_{kj}=0 when $k \neq j$. The studied room was a six-sided, rectangular enclosure with one window and sunlit projection area on the floor. This was ultimately treated as an eight sided enclosure. In matrix form, Equation (10) becomes:

$$\begin{bmatrix} C_1 = a_{11}q_{o,1} + a_{12}q_{o,2} + \ldots + a_{18}q_{o,8} \\ C_2 = a_{21}q_{o,1} + a_{22}q_{o,2} + \ldots + a_{28}q_{o,8} \\ \vdots \\ C_8 = a_{81}q_{o,1} + a_{82}q_{o,2} + \ldots + a_{88}q_{o,8} \end{bmatrix}$$

Solving for the radiosity values results in:

$$[q_{o,k}] = [a]^{-1}[C] \tag{13}$$

The elements of matrix $[q_{o,k}]$ are the final heat fluxes leaving a surface after infinite "inter-reflections" within the interior space, known as surface radiosity. Since the simplified methods result in the net radiation heat transfer, the findings from Equation (13) must also be in terms of a net radiation heat exchange. For an enclosure of N surfaces, the heat balance on any k surface may be expressed as:

$$\frac{Q_k}{A_k} = \left(q_{o,k} - q_{i,k}\right) \tag{14}$$

where A_k is the area of surface k. The right side of Equation (14) is what is comparable to the simplified methods. The incoming flux onto any surface k within the enclosure is expressed as:

$$q_{i,k} = \sum_{j=1}^{N} F_{kj} \cdot q_{o,j} \tag{15}$$

Substituting Equation (15) into (14) gives the net radiation heat transfer between surface k and all other surfaces in an N-surface enclosure:

$$\frac{Q_k}{A_k} = \left(q_{o,k} - \sum_{j=1}^{N} F_{kj} \cdot q_{o,j} \right) \tag{16}$$

The method that was followed to determine relative errors between the simplified methods and the radiosity solutions is the following: (i) specify surface temperatures (ii) increment the surface temperature of the sunlit projection incident on the floor by one degree Kelvin for each run for a parametric comparison (iii) determine the net radiative heat transfer fluxes from simplified methods and from radiosity calculations. For the simplified methods, since fluxes can only be determined between two surfaces, eight equations needed to be carried out (for each method) between the sunlit projection and all other surfaces and then summed to get the net heat transfer of the sunlit projection. For radiosity, equation (16) was utilized. The total flux leaving the sunlit area was found from Eq. (13) and then subtracted from the sum of all other surface fluxes in the enclosure falling on the sunlit area (Eq. (15)). This results in the net radiative heat transfer between the sunlit area and all other surfaces.

3. RESULTS

Results are presented for January 21st at noon and for July 21st at noon. At these times, the sunlit projection areas were 3.172 m^2 and 0.613 m^2 respectfully. Tables 1-2 show the calculated net heat fluxes between the sunlit area and all other room surfaces using the five studied models for the two selected dates. All surfaces were initially set to 290 ^oK and the sunlit area was incremented from 291 ^oK to 310 ^oK, while keeping all other surface temperatures constant. The relative errors of the constant radiative heat transfer coefficient model initially under predict the net heat flux from the sunlit projection when the change in temperature is low. The errors then decrease as the change in temperature increases. The linearized model results in very good results compared to the radiosity model. The non-linear coefficient models result in an effectively constant error compared to the radiosity results. This is due to that these models calculate h_r at each increment in temperature to the fourth power, as does radiosity, while the constant and linearized models do not. The differences are due to the approximations in the emissivity factors especially for the long parallel surface assumption (the radiosity includes all absorption/reflection between all surfaces without approximations). For simple emissivity coefficients, the accuracy is surprisingly good. Two other cases were also analyzed, in that all wall temperatures were set to 290 ^oK, the window temperatures were 275 K in January and 295 ^oK in July, and the sunlit area initially set to 300 ^oK. The sunlit area temperature was then again incremented by 20 ^oK in 1 ^oK increments. The percent errors from these cases in the non-linear methods were negligible.

Table 1: Radiation heat flux between sunlit area and other interior surfaces using the five studied models and comparison with radiosity solution (% relative differences) for January 21st at noon.

ΔT between sunlit area and other surfaces (°K)	Constant coefficients		Linearized coefficients		Non-linear coefficients with approximated emissivity coefficients		Non-linear coefficients with simple emissivity coefficients		Radiosity solutions
	q (W/m^2)	% error	q (W/m^2)	% error	q (W/m^2)	% error	q (W/m^2)	% error	q (W/m^2)
1	5.6	12.5	5.0	0.5	4.5	8.6	5.0	0.5	**5.0**
2	11.2	11.9	10.1	0.5	9.1	8.6	10.1	0.5	**10.0**
3	16.8	11.3	15.2	0.5	13.8	8.6	15.2	0.5	**15.1**
4	22.4	10.8	20.3	0.5	18.5	8.6	20.3	0.5	**20.2**
5	28.0	10.2	25.5	0.5	23.2	8.6	25.5	0.5	**25.4**
6	33.6	9.6	30.8	0.5	28.0	8.6	30.8	0.5	**30.6**
7	39.2	9.1	36.1	0.5	32.8	8.6	36.1	0.5	**35.9**
8	44.8	8.5	41.5	0.5	37.7	8.6	41.5	0.5	**41.3**
9	50.4	7.9	46.9	0.5	42.7	8.6	46.9	0.5	**46.7**
10	56.0	7.4	52.4	0.5	47.7	8.6	52.4	0.5	**52.1**
11	61.6	6.8	57.9	0.5	52.7	8.6	58.0	0.5	**57.7**
12	67.2	6.3	63.5	0.5	57.8	8.6	63.6	0.5	**63.2**
13	72.8	5.8	69.2	0.5	62.9	8.6	69.2	0.5	**68.8**
14	78.4	5.2	74.9	0.5	68.1	8.6	74.9	0.5	**74.5**
15	84.0	4.7	80.6	0.5	73.3	8.6	80.7	0.5	**80.3**
16	89.6	4.1	86.4	0.5	78.6	8.6	86.5	0.5	**86.0**
17	95.2	3.6	92.3	0.4	84.0	8.6	92.4	0.5	**91.9**
18	100.8	3.1	98.2	0.4	89.4	8.6	98.3	0.5	**97.8**
19	106.4	2.6	104.2	0.4	94.8	8.6	104.3	0.5	**103.8**
20	112.0	2.0	110.2	0.4	100.3	8.6	110.4	0.5	**109.8**

Table 2: Radiation heat flux between sunlit area and other interior surfaces using the five studied models and comparison with radiosity solution (% relative differences) for July 21st at noon.

ΔT between sunlit area and other surfaces (°K)	Constant coefficients		Linearized coefficients		Non-linear coefficients with approximated emissivity coefficients		Non-linear coefficients with simple emissivity coefficients		Radiosity solutions
	q (W/m^2)	% error	q (W/m^2)	% error	q (W/m^2)	% error	q (W/m^2)	% error	q (W/m^2)
1	5.6	12.0	5.0	0.1	4.5	9.0	5.0	0.1	**5.0**
2	11.2	11.5	10.1	0.1	9.1	9.0	10.1	0.1	**10.0**
3	16.8	10.9	15.2	0.1	13.8	9.0	15.2	0.1	**15.2**
4	22.4	10.3	20.3	0.1	18.5	9.0	20.3	0.1	**20.3**
5	28.0	9.7	25.5	0.1	23.2	9.0	25.5	0.1	**25.5**
6	33.6	9.2	30.8	0.1	28.0	9.0	30.8	0.1	**30.8**
7	39.2	8.6	36.1	0.1	32.8	9.0	36.1	0.1	**36.1**
8	44.8	8.1	41.5	0.1	37.7	9.0	41.5	0.1	**41.5**
9	50.4	7.5	46.9	0.1	42.7	9.0	46.9	0.1	**46.9**
10	56.0	7.0	52.4	0.1	47.7	9.0	52.4	0.1	**52.4**
11	61.6	6.4	57.9	0.1	52.7	9.0	58.0	0.1	**57.9**
12	67.2	5.9	63.5	0.1	57.8	9.0	63.6	0.1	**63.5**
13	72.8	5.3	69.2	0.1	62.9	9.0	69.2	0.1	**69.1**
14	78.4	4.8	74.9	0.1	68.1	9.0	74.9	0.1	**74.8**
15	84.0	4.2	80.6	0.1	73.3	9.0	80.7	0.1	**80.6**
16	89.6	3.7	86.4	0.0	78.6	9.0	86.5	0.1	**86.4**
17	95.2	3.2	92.3	0.0	84.0	9.0	92.4	0.1	**92.3**
18	100.8	2.7	98.2	0.0	89.4	9.0	98.3	0.1	**98.2**
19	106.4	2.1	104.2	0.0	94.8	9.0	104.3	0.1	**104.2**
20	112.0	1.6	110.2	0.0	100.3	9.0	110.4	0.1	**110.2**

Figure 3 shows the percent sunlit area cover on the floor throughout a typical meteorological year in West Lafayette, Indiana. It is highest in winter months and decreases in transition from spring to summer, then increases in transition from summer to fall/winter. Solar angles determine the window projection: in winter, the sun traverses the sky at a low altitude, thus projecting the window onto the floor further back into the room; in summer, the sun is higher in the sky, so the projection is shorter and falls closer to the window wall.

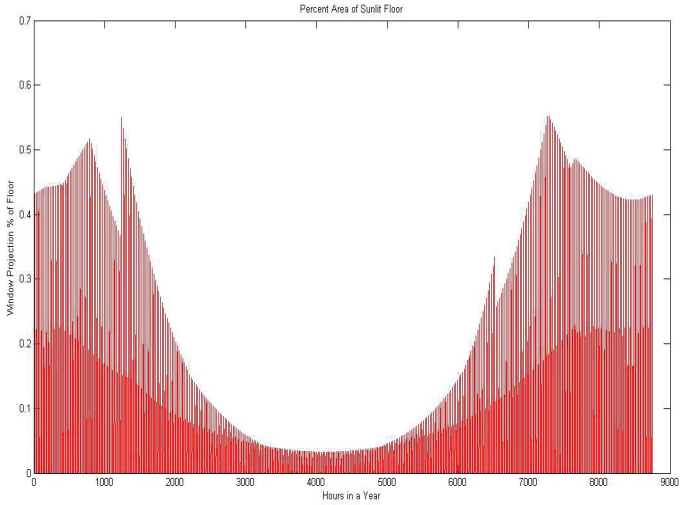

Figure 3: Percent Sunlit Area Cover on Floor (hourly throughout the year).

4. CONCLUSIONS

A radiation exchange model was developed using multiple bounce flux transfer (radiosity) methodology, which predicts either the total flux leaving a surface or the net flux between any surface and all other surfaces in a rectangular enclosure with one window. The heat flux solutions obtained from the radiosity method were then compared to the results using simplified radiant heat transfer models (constant, linearized and non-linear radiative coefficients) for a private office room. The window projection on the floor was computed and treated as a separate surface when using the radiosity method (8-surface enclosure) to evaluate the impact of increased local surface temperatures (due to absorbed solar radiation). In all other models, the room was modeled as a 7-surface enclosure. Results showed that constant and linearized radiation heat transfer coefficients were inaccurate by as much as 12.5% and 0.53% for low temperature changes respectively. This error reduced with increasing temperature differences. The non-linear models with simple emissivity factors proved to be the most accurate, together with some linear models (for specific conditions). The long parallel surface emissivity factor approximation (which is commonly used) results in higher errors (up to 9%). The simplified models result in a quick and generally reasonable prediction of surface fluxes, within a variable temperature range which could however lead to over- or under prediction of heat fluxes and surface temperatures. It should be noted that the results are geometry-dependent: for larger rooms, the view factors and the projected window areas will change and therefore heat fluxes (and surface temperatures) will be different. The model will be further developed and generalized in order to calculate hourly heat fluxes and surface temperatures throughout the year and examine whether a modified simple method can give reliable results overall so that it could substitute the computationally-demanding radiosity modeling.

NOMENCLATURE

ε	emissivity	(unitless)
F_{ij}	view factor from surface *i* to *j*	(unitless)
H	height of window vertice	(m)
h_r	radiation heat transfer coefficient	(W/m^2-^oK)
α	solar altitude angle	(deg)
φ	solar azimuth angle	(deg)

q_{ij}	radiant flux from surface *i* to *j*	(W/m^2)
S	distance from facade	(m)
σ	Stefan-Boltzmann constant	($W.m^2\text{-}^oK^4$)
T	Surface temperature	(^oK)

REFERENCES

Athienitis, A. K., Chen, Y. 2000, The Effect of Solar Radiation on Dynamic Thermal Performance of Floor Heating Systems, *Solar Energy*, vol. 69, no. 3: p. 229-37.

Causone F., Corgnati S.P., Filippi M., Olesen B.W., 2009, Experimental Evaluation of Heat Transfer Coefficients between Radiant Ceiling and Room, *Energy and Buildings*, vol. 41, no. 6: p. 622-28.

Hanibuchi, H.,, Hokoi S., 1998, A Study on Radiative and Convective Heat Exchange In a Room With Floor Heating, In: *Proceedings of IBPSA'98 conference*, International Buildings Performance Simulation Association, Kyoto, Japan.

Olesen, Bjarne 2008, Radiant Floor Cooling Systems, *ASHRAE Journal*, vol. 50, no. 9: p.16-22.

Scheatzle, David 2006, Combining Radiant and Convective Systems with Thermal Mass for a More Comfortable Home, *ASHRAE Transactions*, vol. 112, no. 1: p. 253-68.

Siegel, Robert, Howell, John R., 1972, Chapter 8. Radiation Exchange in an Enclosure Composed of Diffuse-Gray Surfaces, *Thermal Radiation Heat Transfer*, New York: McGraw-Hill.

Siegel, Robert et al. 2010, A Catalog of Radiation Heat Transfer Configuration Factors, *Thermal Radiation Heat Transfer*, 5th ed., New York: CRC, <http://www.engr.uky.edu/rtl/Catalog/tablecon.html#C1>.